All-Optical Switching of an Epsilon-Near-Zero Plasmon in ITO

Justus Bohn (jb933@exeter.ac.uk)
University of Exeter https://orcid.org/0000-0002-1437-6450
Ting-Shan Luk
Sandia National Laboratory
Craig Tollerton
University of Exeter
Sam Hutchins
University of Exeter
Igal Brener
Sandia National Laboratories https://orcid.org/0000-0002-2139-5182
Simon Horsley
University of Exeter https://orcid.org/0000-0001-7242-7941
William Barnes
University of Exeter https://orcid.org/0000-0002-9474-5534
Euan Hendry
University of Exeter

Article

Keywords:

Posted Date: July 23rd, 2020

DOI: https://doi.org/10.21203/rs.3.rs-40947/v1

Version of Record: A version of this preprint was published at Nature Communications on February 15th, 2021. See the published version at https://doi.org/10.1038/s41467-021-21332-y.

All-Optical Switching of an Epsilon-Near-Zero Plasmon in ITO

Justus Bohn[1,*], Ting Shan Luk[2,3], Craig Tollerton[1], Sam Hutchins[1], Igal Brener[2,3], Simon Horsley[1], William L. Barnes[1], and Euan Hendry[1]

[1]School of Physics, University of Exeter, EX4 4QL, UK
[2]Sandia National Laboratories, Albuquerque, 87185, New Mexico, USA
[3]Center for Integrated Nanotechnologies, Sandia National Laboratories, Albuquerque, 87185, New Mexico, USA
[*]jb933@exeter.ac.uk

ABSTRACT

Nonlinear optical devices and their implementation into modern nanophotonic architectures are constrained by their usually moderate nonlinear response. Recently, epsilon-near-zero (ENZ) materials have been found to have a strong optical nonlinearity, which can be enhanced through the use of cavities or nano-structuring. Here, we study the pump dependent properties of the plasmon resonance in the ENZ region in a thin layer of thin indium tin oxide (ITO). Exciting this mode using the Kretschmann-Raether configuration, we study reflection switching properties of a 60 nm layer close to the resonant plasmon frequency. We demonstrate the thermal switching mechanism, which results in a shift in the plasmon resonance frequency of 20 THz for a TM pump intensity of 75 GW/cm^2. For degenerate pump and probe frequencies, we highlight an additional coherent contribution, not previously isolated in ENZ nonlinear optics studies, which leads to an overall pump induced change in reflection from 1 % to 45 %.

Introduction

Nonlinear optics is utilised for a wide range of photonic applications such as quantum all-optical data processing[1,2], information technology[3,4] and telecommunication applications. With the rise of new computational demands such as artificial intelligence, all-optical signal processing is often seen as a breakthrough technology for the next generation of computation and communication devices[5]. However, such applications are limited by the interaction of light signals, with extremely weak optical nonlinearity exhibited by most materials. This leads to high power consumption and a large physical size of optical circuitry, making integration into existing nanophotonic platforms challenging[6,7]. Moreover, most optical switching materials and geometries are not compatible with existing complementary metal–oxide–semiconductor (CMOS) fabrication technologies, which is preferential for implementation into existing platforms[8].

Recently, epsilon-near-zero (ENZ) materials have attracted much attention, not only for their intriguing linear properties[9], but also because they exhibit large optical nonlinearities[10,11]. Moreover, a subset of ENZ materials, transparent conductive oxides, exhibit resonance frequencies in the near-infrared, thereby offering potential for integrated telecom applications[12–17]. Indium-tin-oxide (ITO), as one example, has been shown to undergo a refractive index change of order unity upon optical pumping of a thin film[18]. This effect is thought to arise from electron heating, which leads to a change in effective mass due to the non-parabolic electron dispersion[19]. Similar optical nonlinearities have been measured for doped zinc oxides[20,21] and CdO[22]. These materials are also tuneable, with variability in their doping level, giving control over the ENZ resonance wavelength spanning the infrared range[23,24]. To further increase the optical switching properties of transparent conducting oxides, different strategies have been employed, including additional structuring[16,25,26] or the design of cavity modes[22,27–29].

It is also well known that near the ENZ frequency of a thin transparent conducting oxide one can also excite a plasmon resonance, giving rise to enhancement of the incoming field and near-perfect absorption[30]. We will refer to this resonance as the ENZ plasmon. One can excite plasmons using a high index incident prism in the Kretschmann-Raether configuration, circumventing the need for nano-structuring or the additional support of a cavity. This approach has been employed to study plasmon based nonlinear optical dynamics in gold films[31–33]. However, while ENZ plasmon excitation has been employed to enhance third harmonic radiation[34], there has been no study of all-optical switching in transparent conducting oxides in this desirable geometry.

Here, we investigate optically induced shifting of the ENZ plasmon frequency via pump-probe experiments in the Kretschmann-Raether configuration. This geometry provides a potential switching platform from near-total absorption to total internal reflection upon tuning the plasmon resonance into and out of the spectral range. We identify two contributions to the nonlinear signal: A dominant thermal switching process results in a shift in the plasmon resonance frequency of 20 THz for a

TM pump intensity of 75 GW/cm^2 when pumping resonantly, resulting in a change in reflection of the probe from 1 % to 30 %. Exclusively for the TM pump polarisation, we identify an additional coherent contribution. These two mechanisms combine to enable reflection switching of a 60 nm layer by more than an order of magnitude, with a measured change in reflection of the probe from 1 % to 45 % for a pump intensity of 75 GW/cm^2.

Exciting ENZ plasmons

Wavevector matching is required to excite a plasmon. In our design we follow the Kretschmann-Raether configuration as seen in Figure 1a. The prism enables the pump and probe beams to be incident upon the ITO layer beyond the critical angle, resulting in a wavevector beyond the air light-line and thereby enabling plasmon excitation in the near perfect absorption regime. Of interest here is the area around epsilon being zero, which coincides with the backbended segment of the plasmon dispersion, shown in Figure 1c for a 60 nm thick film (dispersion model found in the supplementary). We refer to this plasmon segment in the remainder of this paper as the ENZ plasmon region. We are specifically interested in the non-radiative ENZ plasmon, which lies beyond the air light line – in this region one expects to observe a near-perfect absorption and enhanced fields[30].

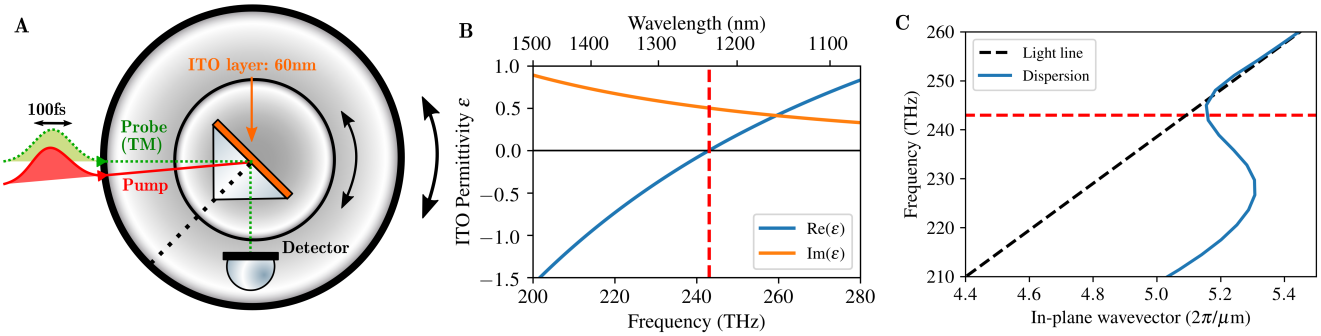

Figure 1. Basic material properties and schematic set-up. a, Schematic pump-probe setup with the ITO sample index matched to a prism in order to probe the ENZ plasmon beyond the critical angle. ($\theta = 45°$) **b**, Optical permittivity of the ITO film used in this study, measured using ellipsometry, with an epsilon-near-zero frequency of 243 THz (red dashed). **c**, Plasmon dispersion branch of the 60 nm ITO thin film closest to the air light line, calculated following supplementary information section S3.

Nonlinearity near ENZ resonance

Recent measurements have shown that pumping below the band-gap of a transparent conducting oxide leads to carrier heating which subsequently results in an increased effective mass and decreased plasma frequency[25]. Such an intensity dependent plasma frequency should materialise as a shifting resonance frequency of an ENZ plasmon. We study this effect in the ENZ plasmon dispersion of a 60 nm ITO thin film using a pump-probe scheme. To begin, we pump with TE polarisation and probe with TM polarisation – this removes coherent interference of pump and probe pulses at the cost of less efficient absorption. Figure 2a shows three typical pump-probe measurements where we pump and probe different regions of the plasmon resonance. For a probe frequency of 240 THz (red, case I) the ENZ resonance red shifts away from the probe, the absorption decreases and we see an increase in reflectivity. For 214 THz (green, case III) the ENZ resonance shifts spectrally towards the probe, the absorption increases and we see a decrease in reflectivity. Both cases display expected temporal dynamics: a fast, $\sim$100 fs (pulse limited) initial change, followed by a slower , $\sim$1 ps thermal relaxation, similar to previous studies[18,20,35]. For 227 THz (orange, case II) the ENZ resonance shifts spectrally through the probe, and we observe some rather unusual dynamics in the pump-probe signal that, to the best of our knowledge, have not previously been observed. To understand these better, we have introduced a dynamic model, which captures effects arising due to rapid time-dependent changes to the phase of reflection (details in supplementary S3). With this model, we can reproduce the features seen in our pump probe signals: the three broad types of behaviour are shown for various frequencies in Figure 2b and modelled using time varying reflection coefficient implied directly from experimental observations. For the first two cases, it is straightforward to define maxima/minima in reflection (R_{pumped}) relative to the initial reflection (R_0), as labelled in Figure 2a. Defining a maximal response in the oscillatory case is problematic - for simplicity, we define $R_{pumped} = R_0 + \Delta R_{max} + \Delta R_{min}$ for all measured time delay scans.

By varying both the incident angle and the degenerate pump/probe frequency, one can observe the plasmon dispersion shift as seen in Figure 2c. Upon illuminating the sample with a TE pump of 75 GW/cm^2 intensity we measure a red-shift of the ENZ plasmon resonance, as seen for the pumped reflection (R_{pumped}) relative to the initial reflection (R_0). We interpret these changes

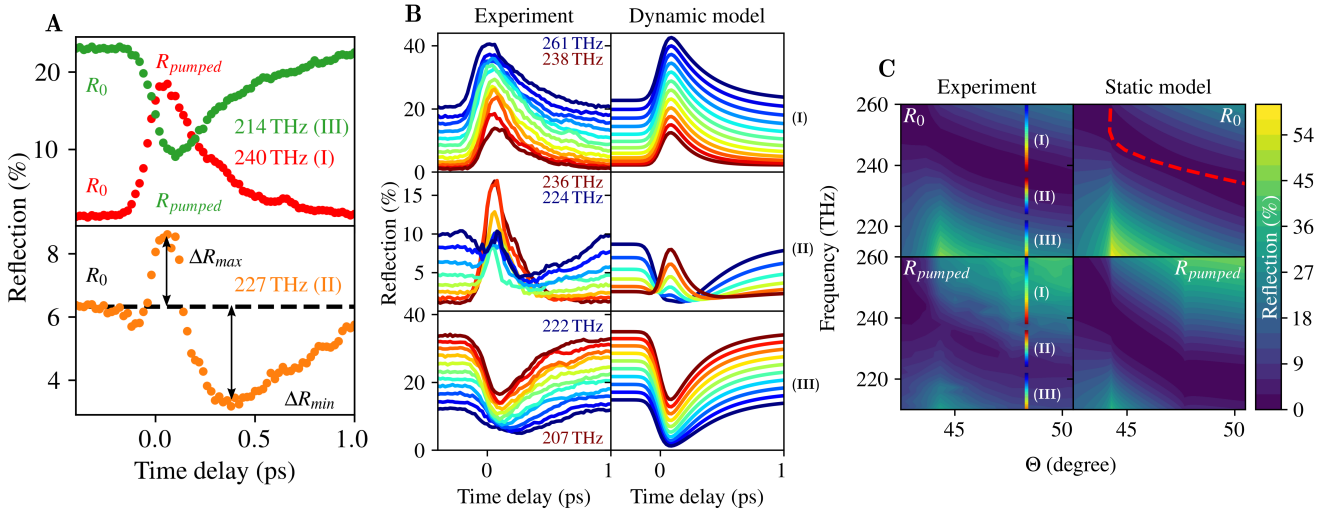

Figure 2. Time dependence of the nonlinear reflection for degenerate pump and probe frequencies. a, Three typical pump-probe measurements, where: I) the probe frequency (240 THz, red) is larger than the plasmon resonance frequency, II) the resonance shifts spectrally through the probe during pumping (227 THz, orange), and III) the probe frequency is smaller than the pumped resonance (214 THz, green). While the probe is TM polarized to study the plasmon response, the 75 GW/cm^2 pump is TE polarized to avoid coherent contributions. The probe angle is 48.3°. **b**, Various pump-probe measurements divided into the previously discussed three case types. The dynamic model shows the reflection coefficient for a time varying effective medium. **c**, Scans of the probe reflection over incoming angle and degenerate frequency, showing the initial R_0 (top) and the pumped case R_{pumped} (bottom). The vertical jet coloured lines at 48.3° indicate the measurements presented in b. The transfer matrix model on the right shows the expected initial reflection at the top with the ENZ plasmon dispersion from Figure 1c (red dashed) with R_{pumped} based on the carrier heating nonlinearity at the bottom (modelling details in S3).

using a simplified "static" model, which calculates the reflection using a transfer matrix model assuming an effective medium with an intensity dependent permittivity for the ITO layer (details in S3, static model). We assume a linear intensity dependent shift of the plasma frequency, $\omega_p(I) = (1 + \omega_{p,2} I)\,\omega_{p,0}$, where I is the calculated absorbed intensity and $\omega_{p,2}$ is the nonlinear fit parameter. This approach gives good agreement for the red-shifting behaviour of the resonance, while also confirming some more subtle features, such as the critical angle feature for the probe pulse just below 45°, as well as a second critical angle feature near 48°, which arises due to the 3.4° difference in angle between pump and probe. We find best agreement with the data for an intensity dependent red-shifting of the plasma frequency, described by $\omega_{p,2} = -0.35\ \%/\frac{\mathrm{GW}}{\mathrm{cm}^2}$. This is the general behaviour expected for heating of the electron plasma in ITO, an effect which arises due to the non-parabolicity of the conduction band in this material[22,36,37]. However, as discussed in supplementary information section S3, comparison between experiment and modelling suggests that the electron heating is weaker in our ITO compared to that previously reported in[36], as our extracted value for $\omega_{p,2}$ is similar despite an increased local intensity arising due to the Kretchman geometry. We do not fully understand this discrepancy, but it may arise due to complications in the homogeneous analysis used in ref[36] (discussed in detail in the supplementary section S3), or due to variations between ITO samples. As further discussed in the supplementary S3, we can not identify changes to the scattering rate as readily as the changes to the plasma frequency, as the scattering rate affects mainly the width of the plasmon resonance, which is impacted by an artefact of our analysis using our static model (discussed below). However, it is expected that heating should have minimal effect on scattering rate in transparent conducting oxides due to the dominance of impurity scattering[19]. As shown explicitly in figure S2, and discussed in the surrounding supplementary text, comparison between our dynamic model and experimental data suggests that pump induced changes to scattering rate are negligible.

Intensity dependence

In Figure 3, we vary pump intensity while fixing the pump frequency to 240 THz and incident angle to just beyond the critical angle of the pump (48.3°). The pump polarization is TE, i.e. non-resonant with the ENZ plasmon. On increasing pump intensity, we observe a clear red shift of the ENZ plasmon, with approximately linear intensity dependence. We also observe a more subtle effect: an apparent slight narrowing of the resonance. This is an artifact of our analysis, arising from the oscillatory features for case II, which become more prominent for increasing intensity. Since we are unable to remove completely these

effects in our static analysis, they give rise to slight distortion of the resonance lineshape for high intensities.

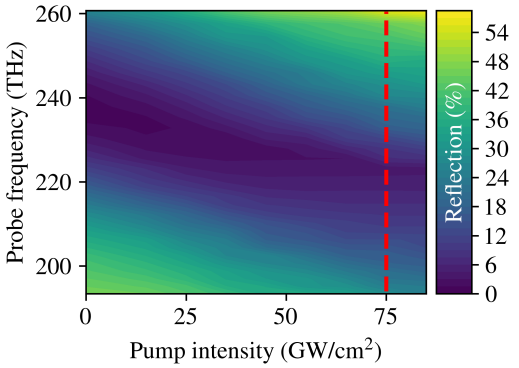

Figure 3. Intensity dependence. Intensity dependent R_{pumped} for a constant incident probe angle of $\Theta = 48.3°$ and a pump with a constant frequency of 240 THz (TE polarized, i.e. non-resonant with the ENZ plasmon). The ENZ plasmon red shifts with increasing pump intensity. The red dashed line indicates the 75 GW/cm^2 used for the measurements in Figure 2.

Coherent vs incoherent response

Finally, we aim to maximize switching: by exciting with a TM pump, a more efficient energy deposition via the ENZ plasmon resonance is expected. We investigate the non-degenerate frequency dependence of the nonlinear material response by fixing the external pump intensity to 75 GW/cm^2 and incident pump angle to 48.3°, and compare TE and TM excitation. Firstly, the pump absorption for TE excitation is only weakly frequency dependent. For this reason, we observe a pump frequency independent shift of the ENZ resonance of 14 THz in Figure 4a. For TM excitation, seen in Figure 4b, we see two additional interesting aspects. For on-diagonal (degenerate) measurements, we can identify a noticeably larger reflection. To our knowledge, this is the first time that a coherent contribution has been distinguished this clearly in a pump-probe measurement on ITO. We note that such coherent effects may be concealed, and not readily separated, within other degenerate pump-probe measurements in the literature. In Figure 4c we compare the coherent and incoherent contributions to our signal. For the non-degenerate case, we observe thermal switching behaviour resulting in a large change in reflection from $R_0 \sim 1$ % to $R_{pumped} \sim 30$ %. This corresponds to a shift of the plasmon resonance frequency of 20 THz, which is more than four times the spectral width of a 100 fs pulse. In the degenerate case, we see a further increase of the differential reflection to $\Delta R \sim 45$ % due to coherent interaction between pump and probe beams. Only by systematically varying both pump and probe frequencies independently have we been able to identify this coherent contribution to switching.

Conclusions

In conclusion, we present an investigation into all-optical switching of ENZ plasmons. We identify two contributions to our nonlinear signal: a thermally driven switching process results in a shift in the plasmon resonance frequency of 20 THz for a pump intensity of 75 GW/cm^2, while an additional coherent contribution is observed for degenerate pump and probe frequencies. In total we observe switching of more than one order of magnitude, from $R_0 \sim 1$ % to $R_{pumped} \sim 45$ % , resulting entirely from resonant conditions allowed by the geometry. For comparison, switching of ITO in air with 75 GW/cm^2 has been shown to result in a change in transmission from 12 % to 34 %[18], for samples with five times the material thickness than those studied here. In addition, switching from near-perfect absorption to high reflection is useful from a signal processing point of view, and could pave the way towards optical plasmon switching at telecom frequencies. Finally, the compatibility with CMOS fabrication technique makes thin TCO layers and their ENZ plasmon feature a compelling new route for nonlinear integrated photonics applications without the need for nanostructure or building additional cavities, while better matching the spatial modes used in photonic circuit systems.

Methods

Numerical simulation and calculation

The plasmon dispersion was calculated using Mathematica 12. The static and dynamic model for the three layer system were calculated using Python 3.7. Details of both models can be found in the supplementary information.

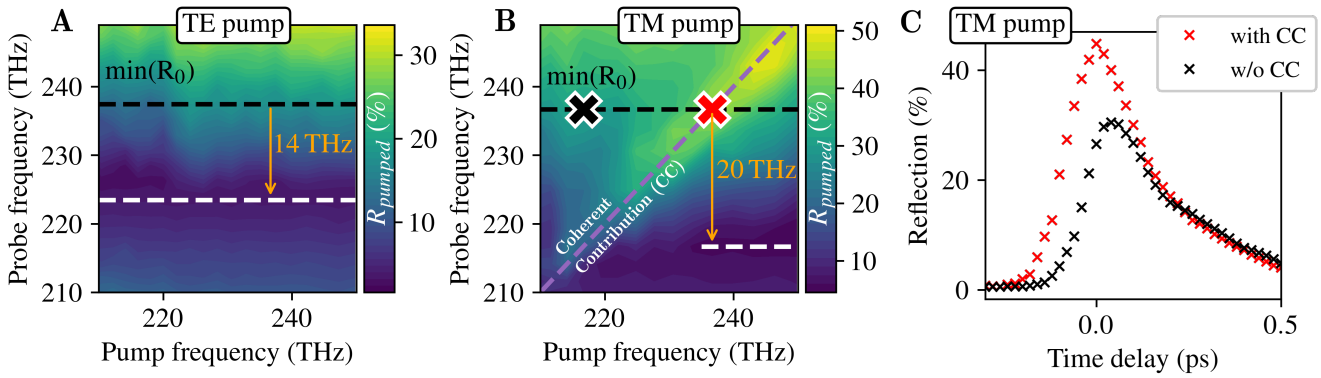

Figure 4. Non-degenerate frequency dependence and coherent contribution. We examine the pump-probe frequency dependence of R_{pumped} for 75 GW/cm^2. **a**, Using a TE pump, the frequency shift of the resonance is 14 THz, and independent of pump frequency. The dashed lines indicate the initial (black) and pumped (white) ENZ plasmon resonance frequency. **b**, A TM pump highlights a coherent contribution (CC) for equivalent polarization and frequency. The higher pump absorption through the plasmon resonance leads to a larger, 20 THz shift of the resonance frequency. Markers indicate the time delay scans compared in **c**, where the probe frequency is 237 THz, while the pump frequency is either 237 THz (red, with CC) or 217 THz (black, without CC).

Sample Fabrication

ITO was sputtered onto cover glass at room temperature using 90/10 In_2O_3/SnO_2 Kurt Lesker target and sputtering tool. The base pressure before deposition was in low 10^{-6} torr, but raised to 3 mT of Ar only during deposition with a RF power of 145 W. In order to achieve high carrier density, both deposition and annealing was performed under in a lowest possible residual oxygen environment. The samples are post-annealed in forming gas for 3 mins at temperatures between 425-525°C in a rapid thermal annealer.

Optical set-up

For the pump-probe measurements, we used an amplified Ti:sapphire laser (Legend Elite, Coherent), with a central wavelength of 800 nm, pulse duration of 100 fs and repetition rate of 1 kHz, feeding two identical OPAs (TOPAS, Light Conversion). The signal output of one OPA was used as the pump, and the signal output of the other OPA was used as the probe, allowing us independent control of pump and probe frequencies. The pump was focused using a 40 cm BK7 lens, the probe with a 25 cm $CaFl_2$ lens. The pump beam diameter (FWHM) was measured to be 800 µm in air, while the probe was 250 µm. To make sure the probes intensity is significantly smaller than the pump we used several additional OD filters to decrease the probe power and tested that the nonlinear reflection was independent of adding/removing filters. We used a referenced tuneable filter wheel to enable a frequency independent pump power. The probe beam was chopped and measured with a fiber connected detector combined with a boxcar and lock-in electronic set-up. The ITO thin layer was positioned on top of a 180 µm coverslip and attached to the front of a right angle prism (EKSMA, UV-FS 5x5 mm) by applying an index matching fluid (Olympus IMMOIL-F30CC). To obtain absolute reflection measurement we used the total internal reflection of a blank coverslip as a reference. The angle of incidence of the pump was set to be $\sim 3.4^\circ$ smaller than that of the probe (5° in air).

References

1. Glezer, E. N. *et al.* Three-dimensional optical storage inside transparent materials. *Opt. Lett.* **21**, 2023, DOI: 10.1364/ol.21.002023 (1996).

2. Cotter, D. *et al.* Nonlinear optics for high-speed digital information processing. *Science* **286**, 1523–1528, DOI: 10.1126/science.286.5444.1523 (1999).

3. Howell, J. C., Bennink, R. S., Bentley, S. J. & Boyd, R. W. Realization of the einstein-podolsky-rosen paradox using momentumand position-entangled photons from spontaneous parametric down conversion. *Phys. Rev. Lett.* **92**, 210403, DOI: 10.1103/PhysRevLett.92.210403 (2004).

4. Leach, J. *et al.* Quantum correlations in optical angle-orbital angular momentum variables. *Science* **329**, 662–665, DOI: 10.1126/science.1190523 (2010).

5. Minzioni, P. *et al.* Roadmap on all-optical processing. *J. Opt. (United Kingdom)* **21**, 063001, DOI: 10.1088/2040-8986/ab0e66 (2019).

6. Makarov, S. V. *et al.* Light-Induced Tuning and Reconfiguration of Nanophotonic Structures. *Laser Photonics Rev.* **11**, 1–25, DOI: 10.1002/lpor.201700108 (2017).

7. Niu, X., Hu, X., Chu, S. & Gong, Q. Epsilon-Near-Zero Photonics: A New Platform for Integrated Devices. *Adv. Opt. Mater.* **6**, 1–36, DOI: 10.1002/adom.201701292 (2018).

8. Miller, D. A. Are optical transistors the logical next step? *Nat. Photonics* **4**, 3–5, DOI: 10.1038/nphoton.2009.240 (2010).

9. Liberal, I. & Engheta, N. Near-zero refractive index photonics. *Nat. Photonics* **11**, 149–158, DOI: 10.1038/nphoton.2017.13 (2017).

10. Reshef, O. *et al.* Beyond the perturbative description of the nonlinear optical response of low-index materials. *Opt. Lett.* **42**, 3225, DOI: 10.1364/ol.42.003225 (2017).

11. Kinsey, N., DeVault, C., Boltasseva, A. & Shalaev, V. M. Near-zero-index materials for photonics. *Nat. Rev. Mater.* **4**, 742–760, DOI: 10.1038/s41578-019-0133-0 (2019).

12. Feigenbaum, E., Diest, K. & Atwater, H. A. Unity-order index change in transparent conducting oxides at visible frequencies. *Nano Lett.* **10**, 2111–2116, DOI: 10.1021/nl1006307 (2010).

13. Ciattoni, A., Rizza, C. & Palange, E. All-optical active plasmonic devices with memory and power-switching functionalities based on ε-near-zero nonlinear metamaterials. *Phys. Rev. A - At. Mol. Opt. Phys.* **83**, 1–8, DOI: 10.1103/PhysRevA.83.043813 (2011).

14. Guo, Q. *et al.* A Solution-Processed Ultrafast Optical Switch Based on a Nanostructured Epsilon-Near-Zero Medium. *Adv. Mater.* **29**, 1–7, DOI: 10.1002/adma.201700754 (2017).

15. Sinatkas, G. & Kriezis, E. E. Silicon-Photonic Electro-Optic Phase Modulators Integrating Transparent Conducting Oxides. *IEEE J. Quantum Electron.* **54**, DOI: 10.1109/JQE.2018.2852144 (2018).

16. Taghinejad, M. *et al.* Hot-Electron-Assisted Femtosecond All-Optical Modulation in Plasmonics. *Adv. Mater.* **30**, 1–7, DOI: 10.1002/adma.201704915 (2018).

17. Qiu, X., Ruan, X., Li, Y. & Zhang, F. Multi-layer MOS capacitor based polarization insensitive electro-optic intensity modulator. *Opt. Express* **26**, 13902, DOI: 10.1364/oe.26.013902 (2018).

18. Alam, M. Z., De Leon, I. & Boyd, R. W. Large optical nonlinearity of indium tin oxide in its epsilon-near-zero region. *Science* **352**, 795–797, DOI: 10.1126/science.aae0330 (2016).

19. Secondo, R., Khurgin, J. & Kinsey, N. Absorptive loss and band non-parabolicity as a physical origin of large nonlinearity in epsilon-near-zero materials. *Opt. Mater. Express* **10**, 1545, DOI: 10.1364/ome.394111 (2020).

20. Kinsey, N. *et al.* Epsilon-near-zero Al-doped ZnO for ultrafast switching at telecom wavelengths. *Optica* **2**, 616, DOI: 10.1364/OPTICA.2.000616 (2015).

21. Caspani, L. *et al.* Enhanced Nonlinear Refractive Index in Epsilon-Near-Zero Materials. *Phys. Rev. Lett.* **116**, 233901, DOI: 10.1103/PhysRevLett.116.233901 (2016).

22. Yang, Y. *et al.* Femtosecond optical polarization switching using a cadmium oxide-based perfect absorber. *Nat. Photonics* **11**, 390–395, DOI: 10.1038/nphoton.2017.64 (2017).

23. Calzolari, A., Ruini, A. & Catellani, A. Transparent Conductive Oxides as Near-IR Plasmonic Materials: The Case of Al-Doped ZnO Derivatives. *ACS Photonics* **1**, 703–709, DOI: 10.1021/ph500118y (2014).

24. Khurgin, J. B. *et al.* Adiabatic frequency shifting in epsilon-near-zero materials: the role of group velocity. *Optica* **7**, 226, DOI: 10.1364/optica.374788 (2020).

25. Guo, P. *et al.* Large optical nonlinearity of ITO nanorods for sub-picosecond all-optical modulation of the full-visible spectrum. *Nat. Commun.* **7**, 12892, DOI: 10.1038/ncomms12892 (2016).

26. Alam, M. Z., Schulz, S. A., Upham, J., De Leon, I. & Boyd, R. W. Large optical nonlinearity of nanoantennas coupled to an epsilon-near-zero material. *Nat. Photonics* **12**, 79–83, DOI: 10.1038/s41566-017-0089-9 (2018).

27. Vassant, S., Hugonin, J.-P., Marquier, F. & Greffet, J.-J. Berreman mode and epsilon near zero mode. *Opt. Express* **20**, 23971, DOI: 10.1364/oe.20.023971 (2012).

28. Newman, W. D. *et al.* Ferrell-berreman modes in plasmonic epsilon-near-zero media. *ACS Photonics* **2**, 2–7, DOI: 10.1021/ph5003297 (2015).

29. Kim, J. *et al.* Dynamic Control of Nanocavities with Tunable Metal Oxides. *Nano Lett.* **18**, 740–746, DOI: 10.1021/acs.nanolett.7b03919 (2018).

30. Campione, S., Kim, I., de Ceglia, D., Keeler, G. A. & Luk, T. S. Experimental verification of epsilon-near-zero plasmon polariton modes in degenerately doped semiconductor nanolayers. *Opt. Express* **24**, 18782, DOI: 10.1364/oe.24.018782 (2016).

31. Exter, M. V. & Lagendijk, A. Ultrashort Surface-Plasmon and Phonon Dynamics. *Phys. Rev.* **60**, 49–52 (1988).

32. Devižis, A., Vaičikauskas, V. & Gulbinas, V. Ultrafast pump-probe surface plasmon resonance spectroscopy of thin gold films. *Appl. Opt.* **45**, 2535–2539, DOI: 10.1364/AO.45.002535 (2006).

33. De Leon, I., Shi, Z., Liapis, A. C. & Boyd, R. W. Measurement of the complex nonlinear optical response of a surface plasmon-polariton. *Opt. Lett.* **39**, 2274, DOI: 10.1364/ol.39.002274 (2014).

34. Luk, T. S. *et al.* Enhanced third harmonic generation from the epsilon-near-zero modes of ultrathin films. *Appl. Phys. Lett.* **106**, DOI: 10.1063/1.4917457 (2015).

35. Elim, H. I., Ji, W. & Zhu, F. Carrier concentration dependence of optical Kerr nonlinearity in indium tin oxide films. *Appl. Phys. B: Lasers Opt.* **82**, 439–442, DOI: 10.1007/s00340-005-2079-8 (2006).

36. Alam, M. Z., De Leon, I. & Boyd, R. W. Large optical nonlinearity of indium tin oxide in its epsilon-near-zero region. *Science* **352**, 795–797, DOI: 10.1126/science.aae0330 (2016).

37. Scalora, M. *et al.* Electrodynamics of conductive oxides: Intensity-dependent anisotropy, reconstruction of the effective dielectric constant, and harmonic generation. *Phys. Rev. A* **101**, 053828, DOI: 10.1103/PhysRevA.101.053828 (2020).

Acknowledgments

We acknowledge financial support from the Engineering and Physical Sciences Research Council (EPSRC) of the United Kingdom, via the EPSRC Centre for Doctoral Training in Metamaterials (Grant No. EP/L015331/1). All data created during this research are openly available from the University of Exeter's institutional repository at ***https://ore.exeter.ac.uk/repository/handle/XXX***. SARH acknowledges funding from the Royal Society RPG-2016-186. This work was performed, in part, at the Center for Integrated Nanotechnologies, an Office of Science User Facility operated for the U.S. Department of Energy (DOE) Office of Science. Sandia National Laboratories is a multimission laboratory managed and operated by National Technology & Engineering Solutions of Sandia, LLC, a wholly owned subsidiary of Honeywell International, Inc., for the U.S. DOE's National Nuclear Security Administration under contract DE-NA-0003525. The views expressed in the article do not necessarily represent the views of the U.S. DOE or the United States Government.

Author Contributions

Justus Bohn, Euan Hendry and William Barnes conceived the idea; Justus Bohn designed and built the experiment with input from Craig Tollerton and Sam Hutchins; Justus Bohn carried out all measurements; Ting Shan Luk and Igal Brener grew and characterized the ITO films; Justus Bohn and Euan Hendry developed and carried out the data analysis; Simon Horsley developed the dynamic model; Justus Bohn and Euan Hendry wrote the manuscript with input from all the authors.

Competing Interests

The authors declare that they have no competing financial interests.

Correspondence

Correspondence and requests for materials should be addressed to Justus Bohn, (email: jb933@exeter.ac.uk).

Figures

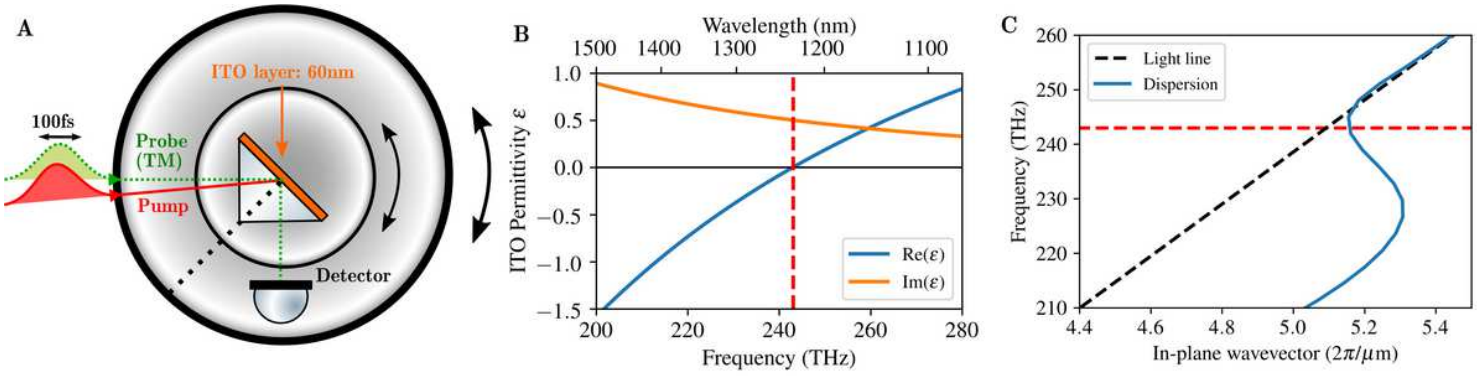

Figure 1

Basic material properties and schematic set-up. a, Schematic pump-probe setup with the ITO sample index matched to a prism in order to probe the ENZ plasmon beyond the critical angle. (θ = 45°) b, Optical permittivity of the ITO film used in this study, measured using ellipsometry, with an epsilon-near-zero frequency of 243 THz (red dashed). c, Plasmon dispersion branch of the 60 nm ITO thin film closest to the air light line, calculated following supplementary information section S3.

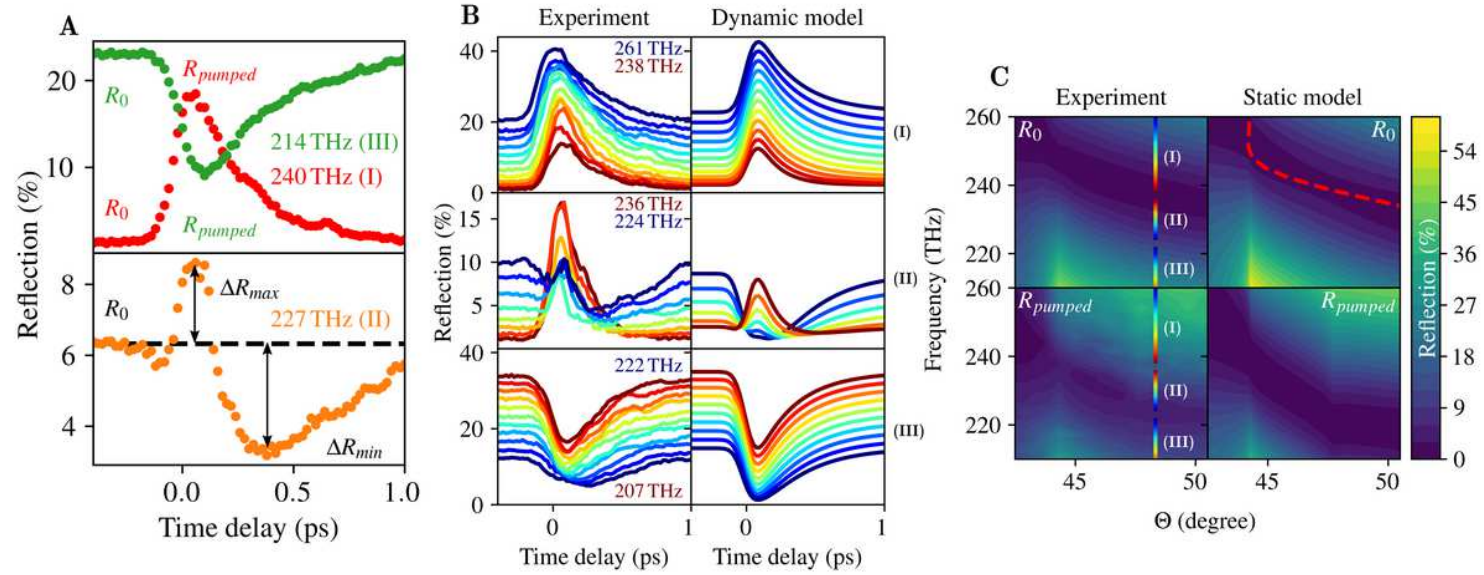

Figure 2

Time dependence of the nonlinear reflection for degenerate pump and probe frequencies. a, Three typical pump-probe measurements, where: I) the probe frequency (240 THz, red) is larger than the plasmon resonance frequency, II) the resonance shifts spectrally through the probe during pumping (227 THz, orange), and III) the probe frequency is smaller than the pumped resonance (214 THz, green). While the probe is TM polarized to study the plasmon response, the 75 GW/cm2 pump is TE polarized to avoid coherent contributions. The probe angle is 48.3° . b, Various pump-probe measurements divided into the previously discussed three case types. The dynamic model shows the reflection coefficient for a time

varying effective medium. c, Scans of the probe reflection over incoming angle and degenerate frequency, showing the initial R0 (top) and the pumped case Rpumped (bottom). The vertical jet coloured lines at 48.3 indicate the measurements presented in b. The transfer matrix model on the right shows the expected initial reflection at the top with the ENZ plasmon dispersion from Figure 1c (red dashed) with Rpumped based on the carrier heating nonlinearity at the bottom (modelling details in S3).

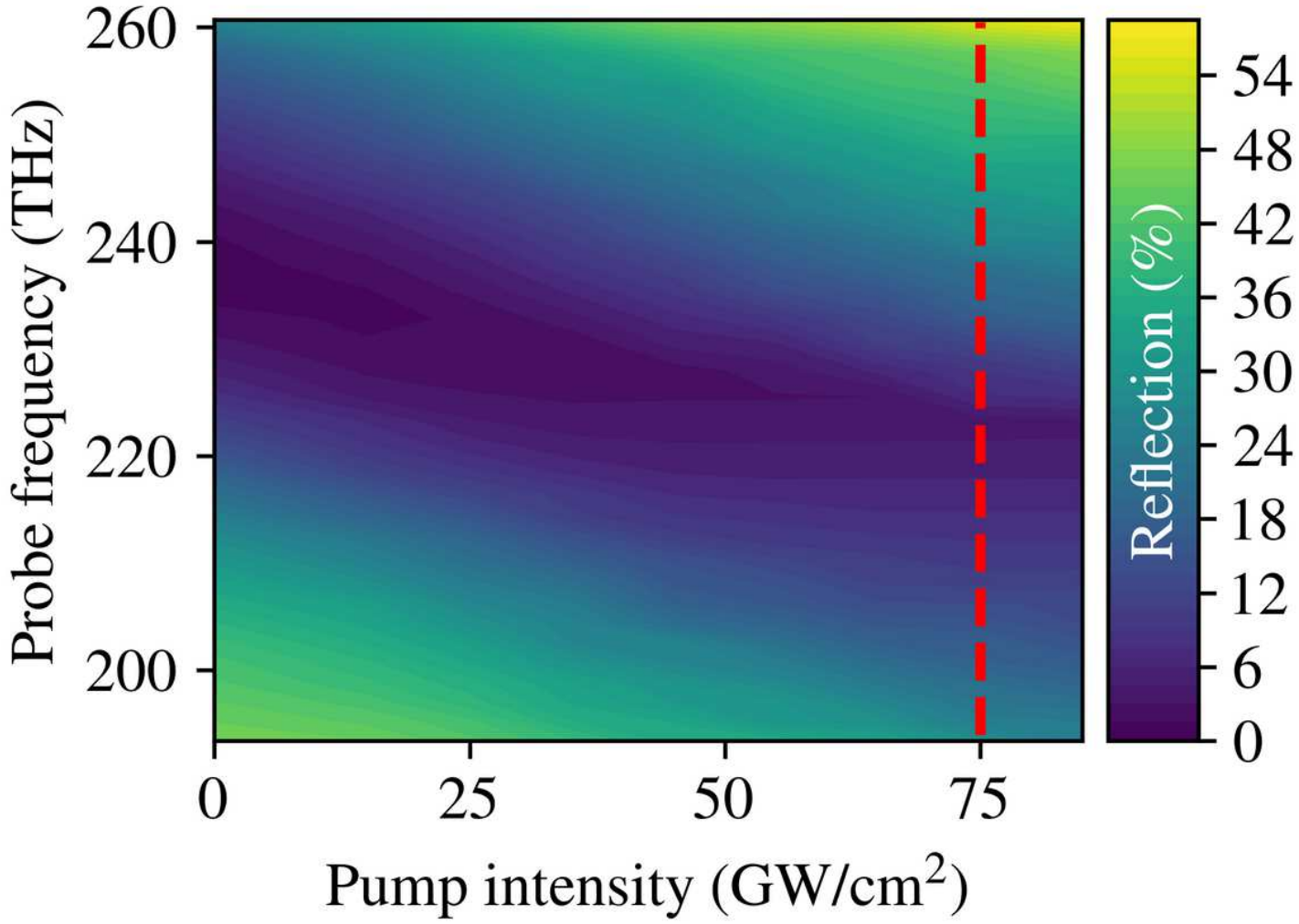

Figure 3

Intensity dependence. Intensity dependent Rpumped for a constant incident probe angle of Θ = 48.3 and a pump with a constant frequency of 240 THz (TE polarized, i.e. non-resonant with the ENZ plasmon). The ENZ plasmon red shifts with increasing pump intensity. The red dashed line indicates the 75 GW/cm2 used for the measurements in Figure 2.

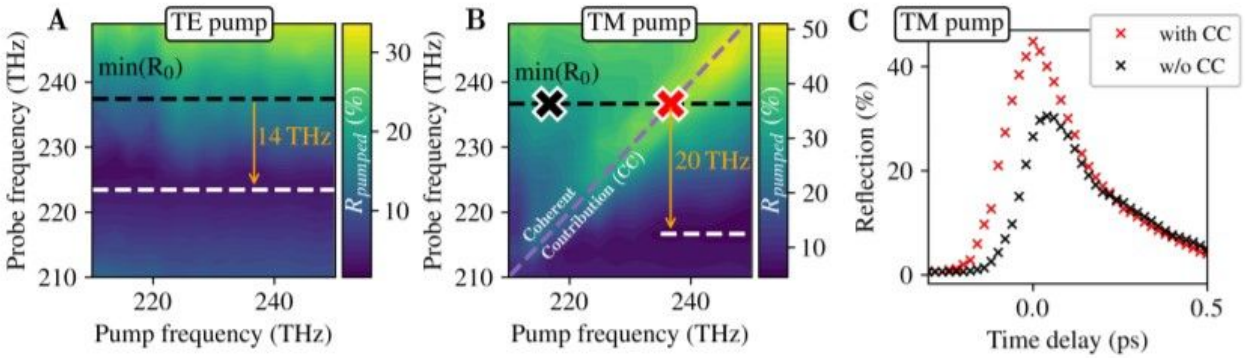

Figure 4

Non-degenerate frequency dependence and coherent contribution. We examine the pump-probe frequency dependence of Rpumped for 75 GW/cm2 . a, Using a TE pump, the frequency shift of the resonance is 14 THz, and independent of pump frequency. The dashed lines indicate the initial (black) and pumped (white) ENZ plasmon resonance frequency. b, A TM pump highlights a coherent contribution (CC) for equivalent polarization and frequency. The higher pump absorption through the plasmon resonance leads to a larger, 20 THz shift of the resonance frequency. Markers indicate the time delay scans compared in c, where the probe frequency is 237 THz, while the pump frequency is either 237 THz (red, with CC) or 217 THz (black, without CC).

Supplementary Files

This is a list of supplementary files associated with this preprint. Click to download.

- sup.pdf